IOPscience iopscience.iop.org

Home Search Collections Journals About Contact us My IOPscience

Drift and clustering of daughter negative ions of H_2O in parent gas

This article has been downloaded from IOPscience. Please scroll down to see the full text article.

2013 J. Phys. D: Appl. Phys. 46 035201

(http://iopscience.iop.org/0022-3727/46/3/035201)

View the table of contents for this issue, or go to the journal homepage for more

Download details:
IP Address: 132.248.33.204
The article was downloaded on 10/12/2012 at 18:34

Please note that terms and conditions apply.

J. Phys. D: Appl. Phys. **46** (2013) 035201 (7pp) doi:10.1088/0022-3727/46/3/035201

Drift and clustering of daughter negative ions of H_2O in parent gas

J de Urquijo[1], A Bekstein[1], G Ruiz-Vargas[1,2] and F J Gordillo-Vázquez[3]

[1] Instituto de Ciencias Físicas, Universidad Nacional Autónoma de México, PO Box 48-3, 62251, Cuernavaca, Mor., México
[2] Facultad de Química, Departamento de Ingeniería Química, Universidad Nacional Autónoma de México, Ciudad Universitaria, 04360, México, D.F., México
[3] Instituto de Astrofísica de Andalucía (IAA–CSIC), PO 3004, 18080 Granada, Spain

Received 17 June 2012, in final form 24 October 2012
Published 10 December 2012
Online at stacks.iop.org/JPhysD/46/035201

Abstract
The mobility of daughter negative ions of H_2O in parent gas has been measured with a pulsed Townsend technique over the density-reduced field strength, E/N, range 9–100 Td and a pressure range 2–16 Torr. It has been found that the mobility of the anions is dependent on the gas pressure. Using a transport theory considering the influence of the permanent dipole field of H_2O, we have found that the pressure-dependent mobilities can be associated with a series of cluster ions of the type $OH^-(H_2O)_n$ ($n = 1$–3), with the mass of the cluster species increasing with the total gas pressure. Also, the mobility of H^- and OH^- could be estimated. Using a Townsend avalanche simulator we have been able to explain the measured ionic currents in terms of an ion–molecule reaction scheme with a single set of swarm and reaction coefficients for each value of the density-reduced field strength, E/N, at several pressures. Regarding the positive ions, the only drifting ion is H_3O^+, the mobility of which could be estimated. The rate constants relative to the formation of the $OH^-(H_2O)_n$ ($n = 1$–3) species were also derived from this study.

(Some figures may appear in colour only in the online journal)

1. Introduction

Studies on atmospheric plasmas are relevant in many areas of basic and applied science as, for instance, to understand the interactions of ions and electrons with atmospheric gases, leading to the formation of ionic cluster species and radicals in the biosphere and in the upper layers of the atmosphere (20–90 km) where transient luminous events (TLEs) take place [1]. On the applied side, many studies and developments are currently carried out on some dielectric barrier plasmas, for example, where H_2O–Ar mixtures are used. This realm of rich and complex plasma chemistry of atmospheric plasmas demands qualitative and quantitative knowledge of the many processes involved in these discharges in which H_2O is involved [1–3]. Particular attention must be paid to cluster formation since water, being a highly polar molecule, can form ion clusters very readily. In spite of the importance of water in many physical phenomena involving its parent and daughter ions, still little is known about their transport and reaction properties. The thorough survey of Viehland up to 1995 [4] reveals this since H_2O does not even appear as a carrier gas on the index lists. One of the problems of studying ion and electron transport in H_2O stems from the fact that water condenses at pressures close to 20 Torr at 293 K.

This paper reports the measurement of the mobility of negative ions in H_2O over a relatively wide range of the density-reduced electric field strength, E/N, from 9 to 100 Td (1 Townsend $= 10^{-17}$ V cm^2), and a gas pressure, p, range extending from 2 to 16 Torr. We have used the pulsed Townsend technique to measure the negative-ion drift velocity and mobility together with an avalanche simulator to help explain the measured transients in terms of known ion–molecule reactions. In particular, the simulations have allowed us to reproduce the temporal evolution of the measured ionic avalanches using self-consistent sets of swarm and reaction data for several pressures at the same E/N value.

 © 2013 IOP Publishing Ltd Printed in the UK & the USA

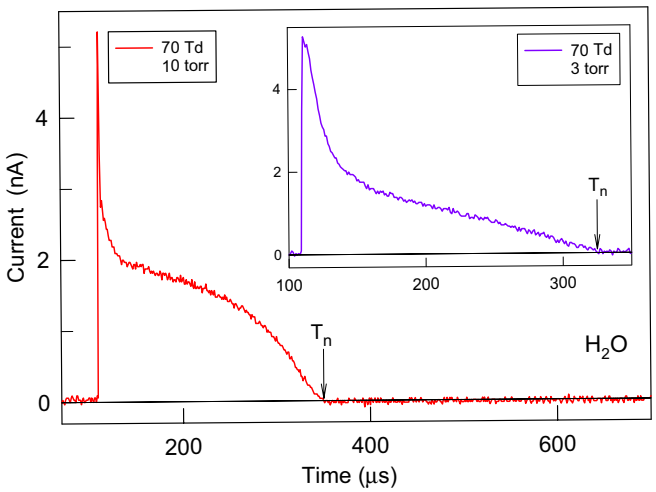

Figure 1. Negative-ion transients in H_2O at $E/N = 70$ Td and pressures of 10 and 3 Torr (inset). The determination of the ionic transit time T_n is indicated by the arrow. The gap distance was $d = 3.1$ cm. The mobilities measured from these pulses are $K_n = 0.69\,\mathrm{cm^2\,V^{-1}\,s^{-1}}$ for $p = 10$ Torr, and $K_n = 0.76\,\mathrm{cm^2\,V^{-1}\,s^{-1}}$ for $p = 3$ Torr. See section 3 for an explanation.

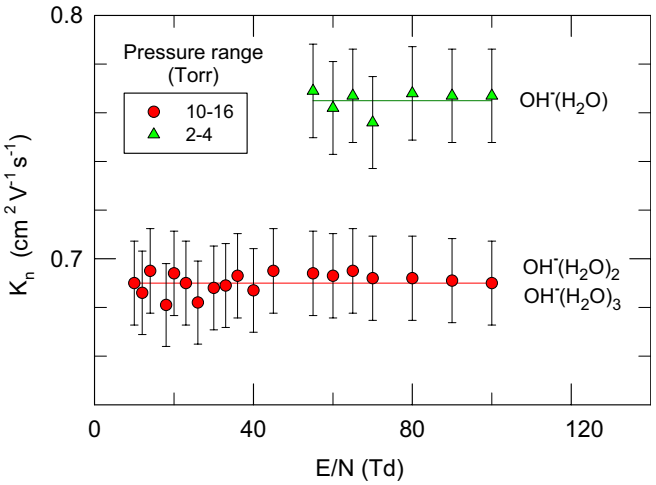

Figure 2. The reduced mobility of negative cluster ions in H_2O as a function of the pressure range. The lines indicate the average value. The negative ions likely to be present in the discharge for each mobility curve are annotated at the right. The size of the error bars is ±2.5%.

2. Experimental details

The pulsed Townsend technique relies on the measurement of the displacement current of ions and electrons through a parallel-plate discharge gap to which an electric field has been applied. A detailed account of the apparatus is given in [5].

The avalanche is started by the incidence of a 3 ns UV laser pulse (Nd : YAG, 355 nm, 4–6 mJ) on the aluminum cathode, liberating photoelectrons that will move towards the anode and react with the gas neutrals during its passage, forming an avalanche pulse bearing a fast, electron component, followed by a slow ionic one. The total current was amplified by a transimpedance amplifier of $10^7\,\mathrm{V\,A^{-1}}$ with a bandwidth of 400 kHz. All the measurements were carried out at room temperature (291–301 K) and water vapour pressures below saturation (about 20 Torr). High purity water (Sigma Aldrich) was used throughout.

Figure 1 shows two representative ionic transients in H_2O at $E/N = 70$ Td and pressures of 10 and 3 Torr (inset). The particular purpose of this example is to show the remarkable difference in the measured mobility since, as will be discussed at length in section 3, the negative-ion mobility in H_2O is strongly dependent on pressure. The initial rise, due to the electrons, is followed by a rather fast decay, lasting 10–15% of the ionic drift time, T_n, is most likely due to ion–molecule reactions that lead finally to the formation of a majority ionic species moving towards the anode with a drift time T_n. This issue will be discussed at length in further sections of this paper. Having determined T_n, the drift velocity is evaluated as

$$v_n = d/T_n, \tag{1}$$

where d is the drift distance. Once v_n has been determined, the reduced mobility is calculated from the expression

$$K_n = \frac{v_n}{N_0(E/N)}. \tag{2}$$

The ionic avalanche pulses shown in figure 1 cannot be analysed in terms of the simple analysis that considers a single species drifting across the discharge gap without reacting with the gas molecules during its passage through the discharge gap. As will be discussed in section 3, the ions drifting under the conditions of this experiment are the result of a dissociative electron attachment process leading to the formation of, predominantly, H^-, which reacts rapidly with the H_2O neutrals to form OH^-, followed by ion–molecule reactions leading to the formation of cluster ions of the type $OH^-(H_2O)_n$ ($n \geqslant 1$) [6–8].

In order to have a well-defined pulse shape due to the negative ions moving in the discharge gap all mobility measurements were limited to an upper E/N value of 100 Td, that is, slightly below the critical value where the ionization (α) and attachment (η) coefficients are equal [9] since (a) for $\eta > \alpha$, in the pulsed Townsend experiment the contribution of the negative-ion current is predominant, as is shown in figure 1 and, (b) the interpretation of the ion signals becomes simpler when attachment overwhelms ionization. In this case, α and η pertain to H_2O.

The mobility of the H_2O negative ions, K_n, in H_2O was measured over the pressure range 2–16 Torr. We found a well-defined dependence of K_n with pressure which, within the uncertainty limits of ±2.5–3%, has been grouped in two sets, as is shown in figure 2. The first set, corresponding to the pressure regime 10–16 Torr, has a mobility $K_n = 0.69 \pm 0.02\,\mathrm{cm^2\,V^{-1}\,s^{-1}}$, covering a wide range of E/N from 9 to 100 Td. The second set, corresponding to the pressure range 2–4 Torr, has a mobility $K_n = 0.76 \pm 0.02\,\mathrm{cm^2\,V^{-1}\,s^{-1}}$.

Lowke and Rees [10] used a time-of-flight drift tube to measure the mobility of negative ions in H_2O over the pressure range 1 to 14 Torr at 293 K and covering an E/N range of 4.5 to 120 Td over which they found a single ionic species with a constant mobility of $0.67\,\mathrm{cm^2\,V^{-1}\,s^{-1}}$ (±1%) over the whole E/N range. They assumed that the negative ion in question was H^-. Lowke's measurements are fairly similar to ours both

in pressure and E/N ranges, and their single mobility value is only 3% smaller than ours over the 10–16 Torr range. Henson [11] used a time-of-flight apparatus to measure the mobility of positive and negative ions in saturated H_2O vapour over the temperature range 293–343 K. Our value over the 10–16 Torr range is 30% higher than that of Henson, who assumes that the mass unidentified ions are $OH^-(H_2O)_n$, without assessing the values of n.

3. Reactions

Negative ions of H_2O are formed by dissociative attachment [12–14], leading to the formation of the H^-, O^- and OH^- fragments, all with a threshold around 5.5 eV, and with H^- as the majority fragment anion, with a cross section $\sigma_{DA}(H^-)$ peaking at 6.5×10^{-18} cm^2 at the first decomposition channel with an electron energy of 6.5 eV, while $\sigma_{DA}(O^-)$ and $\sigma_{DA}(OH^-)$ are 10^{-19} cm^2 and 1.2×10^{-19} cm^2, respectively. The second decomposition channel occurs at 8.6 eV with $\sigma_{DA}(H^-, O^-, OH^-)$ values of $(15, 2.8, 0.8) \times 10^{-19}$ cm^2, respectively; in the third channel, O^- formation peaks at 11.8 eV with $\sigma_{DA} = 5 \times 10^{-19}$ cm^2, respectively, while the other two channels have a σ_{DA} that is nearly one order of magnitude smaller. Since the mean energy of electrons in H_2O ranges between 0.04 and 3 eV over the corresponding E/N range 10–100 Td [15], then it is likely that the 6.5 eV dissociative channel be the most relevant, with H^- as the predominant ion species. Once H^- is formed via the reaction

$$e + H_2O \rightarrow H^- + OH \quad (3)$$

it reacts with H_2O, forming OH^- as the main important product via the process

$$H^- + H_2O \rightarrow OH^- + H_2. \quad (4)$$

Betowski *et al* [16] reported two different rate constants of 5×10^{-11} cm^3 s^{-1} and 3.8×10^{-9} cm^3 s^{-1} for reaction (4) from independent flowing afterglow experiments performed in 1971 and 1975, respectively; however, in our study we have found values of this rate constant in the range 10^{-13}–10^{-12} cm^3 s^{-1}, and depending on E/N as is shown in figure 3. Further three-body collisions of OH^- with H_2O result in the formation of cluster anions of the type $OH^-(H_2O)_n$ ($n \geqslant 1$) by the process [17, 18]

$$OH^- + 2H_2O \rightarrow OH^-(H_2O) + H_2O, \quad (5)$$

$$OH^-(H_2O) + 2H_2O \rightarrow OH^-(H_2O)_2 + H_2O, \quad (6)$$

and

$$OH^-(H_2O)_2 + 2H_2O \rightarrow OH^-(H_2O)_3 + H_2O. \quad (7)$$

As regards the positive ions, it is well known that several ion species may form, depending on E/N and pressure conditions. An inspection to the recommended ionization cross sections states that the collision process

$$e + H_2O \rightarrow H_2O^+ + 2e \quad (8)$$

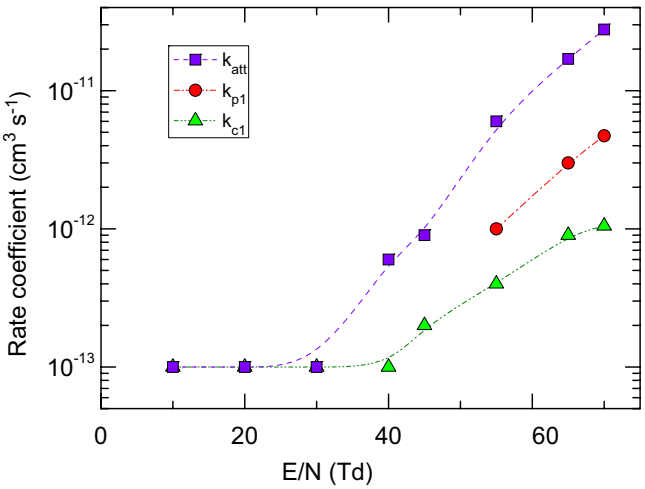

Figure 3. Rate constants for ionization (k_{p1}, reaction (8)), attachment (k_{att}, reaction (3)) and OH^- formation (k_{c1}, reaction (4)) in H_2O as a function of E/N.

is predominant over the energy range 13.5–22 eV [14], followed by the formation of OH^+ with cross sections smaller by two or more orders of magnitude. A calculation of the electron distribution function [19] indicates that electron energies over the above range may be achieved for $E/N >$ 50 Td. Once H_2O^+ is formed, under the present conditions of E/N and pressure it reacts with H_2O to form H_3O^+ via the proton transfer reaction

$$H_2O^+ + H_2O \rightarrow H_3O^+ + OH, \quad (9)$$

which proceeds with a large rate constant of 10^{-9} cm^3 s^{-1} [20]. Below we shall show that this very large value ensures that H_2O^+ is rapidly converted into H_3O^+, hence we shall assume that the only positive ion under the present conditions is H_3O^+. Finally, the ion–ion recombination reaction

$$H_3O^+ + OH^-(H_2O) \rightarrow 3H_2O \quad (10)$$

deserves attention since it has a very fast rate constant of $k_{i-i} = 10^{-6}$ cm^3 s^{-1} [21]. Let us assume that the discharge volume is a 3.1 cm^3 cylinder of 1 cm^2 base and 3.1 cm height. With an initial photoelectron number of $\sim 10^6$, and for $E/N \leqslant$ 70 Td, let us say that 30% of the total number of charged particles ($\alpha < \eta$) correspond to H_3O^+, hence we have a density of $\sim 10^5$ H_3O^+ ions per cm^3, and the recombination frequency would be $\sim 10^5 k_{i-i} = 0.1$ s^{-1}. On the other hand, over the present pressure range 2–16 Torr ($N = 6.6 \times 10^{16}$–5.3×10^{17} cm^{-3}) the conversion frequency for reaction (6) would be $k_{c1}N^2 = 6.6 \times 10^4$–$5.3 \times 10^5$ s^{-1}, after taking the highest value for k_{c1} from figure 3. Notwithstanding that these values are order-of-magnitude approximations, one sees clearly that ion–ion recombination can be safely ignored under the present experimental conditions. Thus, in what follows the reaction scheme that we shall use is that represented by reactions (3) to (9).

Because of the high gas pressures used in our experiment, no mass spectrometry analysis is present. Hence, ion identification should be carried out through indirect means.

Provided that H_2O is a highly polar molecule with a permanent dipole moment $\mu = 1.8$ D, and a dipole polarizability $\alpha_d = 1.45 \times 10^{-24}$ cm^3, ion identification is impractical by resorting to a comparison with the value calculated from the so-called Polarization limit formula from Langevin [22]

$$K_{pol} = \frac{13.56}{\sqrt{m_r \alpha_d}}, \tag{11}$$

where m_r is the reduced mass of the negative ion and H_2O in amu, and α_d is the dipole polarizability in Å^3. K_{pol} is calculated from equation (11) in units of cm^2 V^{-1} s^{-1}.

A good summary and discussion of more accurate mobility theories has been discussed by de Gouw *et al* [23], who have presented a comprehensive review of transport theories that consider the ion-induced dipole interaction together with the effects of the ion–permanent dipole interaction, the latter being absent in Langevin's formula. In the paper of Gouw *et al* [23], a single plot of the ratio between the low-field mobility due to the permanent dipole and ion-induced dipole interaction K_{00}, and Langevin's mobility K_{pol}, as a function of the ratio $\mu/\alpha_d^{1/2}$ is provided, from which the mass of the ion in question can be inferred. The ratio $\mu/\alpha_d^{1/2}$ is a measure of the importance of the permanent dipole interaction. For the case of negative ions in H_2O, $\mu/\alpha_d^{1/2} = 1.54 \times 10^{12}$ D cm$^{3/2}$. Figure 3 of de Gouw's paper is a plot of the ratio between the low-field mobility K_{00}—which we have measured, in this case—and the polarization limit mobility K_{pol} as a function of $\mu/\alpha_d^{1/2}$. Furthermore, resorting to the more comprehensive theory of Barker and Ridge [24], who assumed that the polar molecule rotates freely during the collision, and averaged the ion–dipole interaction potential over all angles, we found that the measured values for the ratio $K_{00}/K_{pol} = 0.23$ fit in well for the two groups of ionic mobilities in H_2O for the $OH^-(H_2O)$ species over the pressure range 2–4 Torr, while the anions $OH^-(H_2O)_2$ and $OH^-(H_2O)_3$ do so over the 10–16 Torr range, since their mobilities lie well within quoted uncertainties. Wilson *et al* [18] report the presence of substantial amounts of $OH^-(H_2O)_n$ ($n = 1$–6) from a time-of-flight/mass spectrometer experiment, operated with a pulsed discharge in H_2O at a pressure of 1 Torr. In spite of the pulsed character of this experiment, no measurements of the negative-ion mobilities were reported by this author.

The present pressure range was limited at the upper end by the H_2O vapour saturation pressure, and at the lower end by the difficulties in achieving good signals, since, as was noted, negative-ion formation in H_2O proceeds dissociatively with a threshold of about 5.5 eV, thereby limiting the exploration for $E/N \geqslant 10$ Td. The upper E/N range was limited to 100 Td in order to ensure that the pulse shapes were mostly due to negative ions since the critical value of E/N for H_2O is $E/N_{crit} \approx 130$ Td [9].

4. Simulation of the negative-ion avalanche pulses

The simulator used to calculate the density of the charge carrier species solves a set of partial differential equations, using a first-order finite difference approximation. This one-dimensional simulation code also calculates the individual currents of the charged carriers and the total, measurable current in the external circuit that will be used for direct comparison with the transient waveforms obtained from the pulsed Townsend experiment. For a thorough description the interested reader is referred to [25, 26].

Table 1. Values of ionic mobilities in H_2O.

Ion	Source	K_0	Uncertainty
H^-	Theory [23]	2.68	—
OH^-	Theory [23]	0.88	—
H_2O^+, H_3O^+	Theory [23]	0.86	—
$OH^-(H_2O)$	Measurement	0.76	2.5–3%
$OH^-(H_2O)_2$	Measurement	0.71	2.5–3%
$OH^-(H_2O)_3$	Measurement	0.69	2.5–3%

The set of continuity equations of the charged carrier species of linear density n_i involved in the present reaction scheme is

$$\text{Electrons} \quad \frac{\partial n_e}{\partial t} + v_e \frac{\partial n_e}{\partial x} = (k_{ion} - k_{att}) N n_e \tag{12}$$

$$H^- \quad \frac{\partial n_{n1}}{\partial t} + v_{n1} \frac{\partial n_{n1}}{\partial x} = (k_{att} - k_{c1}) N n_1 \tag{13}$$

$$OH^- \quad \frac{\partial n_{n2}}{\partial t} + v_{n2} \frac{\partial n_{n2}}{\partial x} = k_{c1} N n_1 - k_{c2} N^2 n_{n2} \tag{14}$$

$$OH^-(H_2O) \quad \frac{\partial n_{n3}}{\partial t} + v_{n3} \frac{\partial n_{n3}}{\partial x} = (k_{c2} n_{n2} - k_{c3} n_{n3}) N^2 \tag{15}$$

$$OH^-(H_2O)_2 \quad \frac{\partial n_{n4}}{\partial t} + v_{n4} \frac{\partial n_{n4}}{\partial x} = (k_{c3} n_{n3} - k_{c4} n_{n4}) N^2 \tag{16}$$

$$OH^-(H_2O)_3 \quad \frac{\partial n_{n5}}{\partial t} + v_{n5} \frac{\partial n_{n5}}{\partial x} = k_{c4} N^2 n_{n4} \tag{17}$$

$$H_2O^+ \quad \frac{\partial n_{p1}}{\partial t} - v_{p1} \frac{\partial n_{p1}}{\partial x} = (k_{p1} n_e - k_{p2} n_{p1}) N \tag{18}$$

$$H_3O^+ \quad \frac{\partial n_{p2}}{\partial t} - v_{p2} \frac{\partial n_{p2}}{\partial x} = k_{p2} N n_{p1}. \tag{19}$$

Electron and ion diffusion (longitudinal) effects are practically uninfluential on the shape of the ionic components, hence we have ignored them altogether in order to simplify the already complex task of solving the set of coupled equations (12)–(19).

The total current is calculated from

$$I_{Tot}(t) = \sum_i \frac{q_i}{T_i} \int_0^z n_i(z,t)\, dz, \tag{20}$$

where $T_i = d/v_i$ is the transit time and v_i is the drift velocity.

The simulations were performed for selected E/N values over the range 10–70 Td. The upper limit was selected as that where the ionization coefficient α becomes about one-tenth of the attachment coefficient η, since the contribution of the positive ions becomes more influential on the pulse shapes.

As stated above, the mobility of the $OH^-(H_2O)_n$ ($n = 1,3$) ions was determined directly from the curve fitting procedure. The mobility of OH^-, OH^-, H_2O^+ and H_3O^+ was estimated from the procedure outlined above [23]. The values of these

Table 2. Values of the rate constants.

Parameter	Reaction	Source	Value	Δ[a]	Comments
k_{p1} (α/N)	(8)	[15, 19]	Figure 3	±5%	H_2O^+ formation
k_{p2}	(9)	[16]	10^{-9} [b]	—	H_3O^+ formation
k_{att} (η/N)	(3)	[15, 19]	Figure 3	±5%	H^- formation
k_{c1}	(4)	This work	Figure 3	±50%	OH^- formation
k_{c2}	(5)	This work	8×10^{-30} [c]	±50%	OH^- (H_2O)
k_{c3}	(6)	This work	2.5×10^{-31} [c]	±50%	OH^- $(H_2O)_2$
k_{c4}	(7)	This work	1.5×10^{-31} [c]	±50%	OH^- $(H_2O)_3$

[a] Δ is the uncertainty.
[b] Two-body reaction in units of $cm^3\ s^{-1}$.
[c] Three-body reactions in units of $cm^6\ s^{-1}$.

mobilities are summarized in table 1. Table 2 contains the values of the swarm parameters and reaction rate constants used or derived from the simulation procedure. The electron drift velocity, v_e, was taken from [15] and the rate constants for ionization k_{p1} (equations (12) and (18)) and attachment k_{att} (equations (12) and (13)) were calculated from values of the ionization (α) and attachment coefficients (η) as $k_{p1} = \alpha v_e$ and $k_{att} = \eta v_e$. In the absence of published values of α and η these were calculated with the Bolsig+ code [19]; the resulting effective attachment coefficient ($\alpha - \eta$) was normalized to that measured [9] and then the final values of α and η were normalized accordingly. Variations of ±5% around these values for $E/N \geqslant 30$ Td were allowed during the fitting procedure; however, for $9 \leqslant E/N \leqslant 70$ Td the final η/N values turned out to be up to four times higher than those estimated from the Bolsig+ code.

The rate constant k_{c1} for conversion of H^- into OH^- (reaction (4)) was determined from curve fitting to the ionic pulses. This rate was found to be about three orders of magnitude smaller than that reported [16], systematically dependent on E/N, and is plotted in figure 3. In the absence of any published values for the reaction rate constants k_{c2} to k_{c4} (reactions (5)–(7), respectively), we also derived their values from curve fitting to the ionic transients. In this respect it was very helpful to have measured the ionic currents at several pressures since only a single value of these rate constants was used to fit all transients at the same E/N value, thereby having a reliable self-consistent set of reaction and mobility data. As a matter of fact, we did not find any E/N dependence of these rate constants. Finally, the reaction rate constant for H_3O^+ production (reaction (9)) was taken from Albritton [16] and Anicich [20].

Figure 4 shows the simulation of the early evolution of the currents due to electrons and ions during the first 2 μs for an ionic avalanche pulse at $E/N = 70$ Td and $p = 10$ Torr. For the sake of clarity both axes are logarithmic. The electrons predominate in the discharge gap over most of their first transit time ($T_e \approx 500$ ns). It is worthwhile noting the fast growth of the H_3O^+ species is concomitant with the disappearance of the parent H_2O^+ ion. It is also noted that H^- and OH^- form rapidly and start decaying in favour of the cluster species $OH^-(H_2O)_n$ ($n = 1, 3$).

A series of sample ionic avalanches is shown at the same E/N value and different pressures, starting with that of figure 5, for $E/N = 70$ Td and $p = 16$ Torr, together

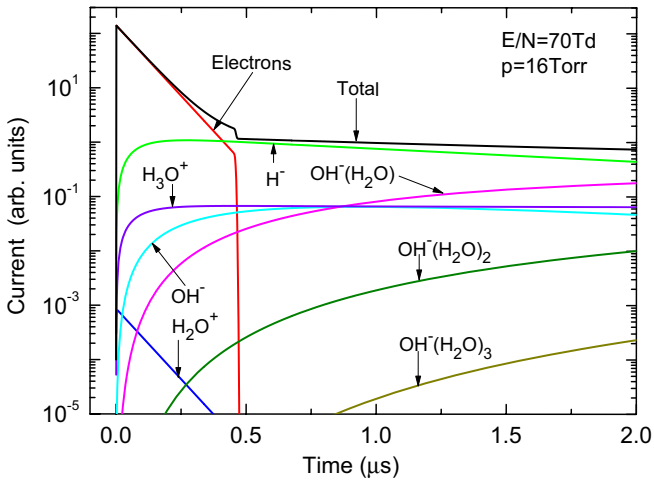

Figure 4. The early evolution of the currents due to electrons and ions during the first 2 μs for an ionic avalanche pulse at $E/N = 70$ Td and $p = 16$ Torr. For the sake of clarity note that both axes are logarithmic.

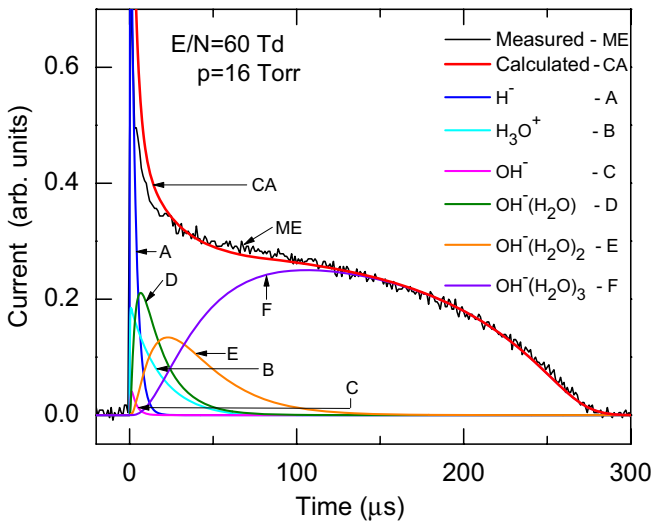

Figure 5. The evolution of the currents of electrons and ions, the ionic avalanche in H_2O at $E/N = 60$ Td and $p = 16$ Torr.

with the corresponding measured pulse for comparison. One can see here that the structures of the pulse are well reproduced, especially that pertaining to $OH^-(H_2O)_3$, which is practically the only ionic species present for $t > 150\ \mu$s. In this simulation one can also observe very clearly how the $OH^-(H_2O)_n$ ($n = 0$–2) species grow and decay, leaving

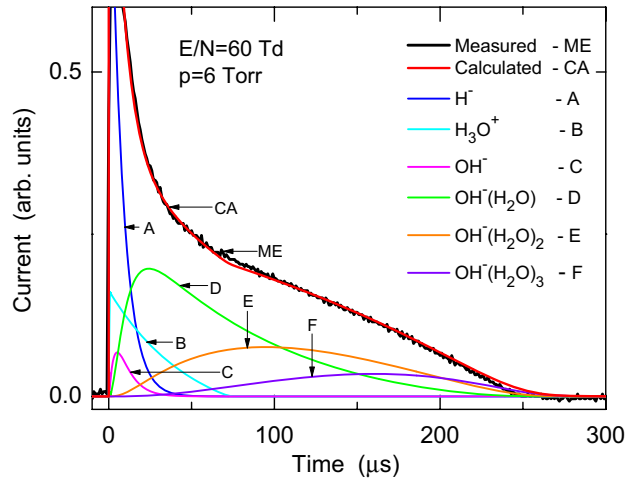

Figure 6. The ionic avalanche in H_2O at $E/N = 60$ Td and $p = 6$ Torr, illustrating the case of an intermediate pressure where no predominant ion species can be assessed during the final stages of ion drift.

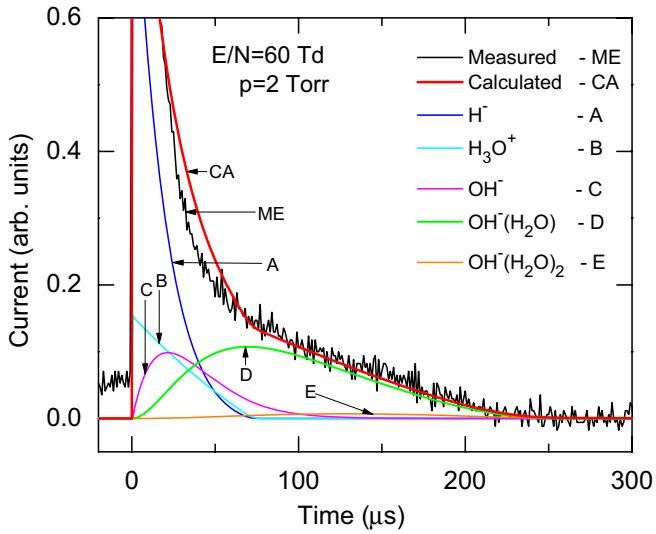

Figure 7. The ionic avalanche in H_2O at $E/N = 60$ Td and $p = 2$ Torr, illustrating the case of a pressure at which the $OH^-(H_2O)$ species is predominant.

eventually $OH^-(H_2O)_3$ in the discharge gap as the only species. Note also that at this pressure the original radical ionic species OH^- disappears very quickly over the first 20 μs. As stated above, a pressure of 16 Torr was the highest used in our measurements in order to preclude any trace of H_2O saturation that would impair the assessment of E/N.

The second simulation shown in figure 6 corresponds to the same E/N value of 60 Td at a pressure of 6 Torr. We consider this pressure value as intermediate since both $OH^-(H_2O)_2$ and $OH^-(H_2O)_3$ compete with almost equal amounts to the final portion of the pulse, thereby making it difficult to assess a predominant ion since the mobilities of these two species are very similar (see table 1). The excellent agreement between measurement and calculation is noteworthy.

The last example of this series with fixed E/N and variable pressure corresponds to figure 7 for the case $E/N = 60$ Td and $p = 2$ Torr, the lowest pressure used in our measurements. Interestingly, one can see here that the predominant ionic species becomes $OH^-(H_2O)$, with only a trace of $OH^-(H_2O)_2$. As expected, OH^- lives longer as the pressure is reduced. Note that even though over the time interval 20–60 μs the fit is only fair, it does preserve the structure. Better improvements can be achieved through minor adjustments to the set of swarm parameters; nevertheless, we have kept these fixed in order to show that all the basic structures of the three pulses over the whole range of measurement are well reproduced with a single set of data.

Note that H_3O^+ disappears rather quickly, and that its contribution, although important, only helps explaining the early fall of the pulse. Even though the positive-ion chemistry was more involved, its overall contribution would still be relatively small since $\alpha \approx 0.1\eta$ at $E/N = 60$ Td.

Thus far we have shown in figures 5 to 7 examples of measured pulsed at fixed E/N and variable pressure. In order to further demonstrate the consistency of the proposed reaction model, figures 8(*a*) to (*d*) illustrate the case of varying E/N while keeping the pressure constant. Despite the fair agreement between simulations and measurements seen in figures 8(*a*) and (*b*), one observes that, again, the structures of the pulse are well reproduced, and that the agreement in figures 8(*c*) and (*d*) is excellent.

5. Discussion

We have presented a comprehensive measurement of the mobility of H^-, OH^-, $OH^-(H_2O)_n$ ($n = 1$–3) and of H_3O^+ in H_2O over a wide range of E/N and pressures, a parameter on which there is scarce information in the literature in pure H_2O in spite of its importance. The most significant feature of these measurements is the strong dependence of the ion mobilities with gas pressure, which is in turn related to the highly polar character of the H_2O molecule to form clusters readily. In spite of the limitations of the experiment regarding mass analysis, the application of an adequate transport theory that considers the permanent dipole interaction has been useful to infer the identity of the various ionic species drifting in pure H_2O. These findings may explain the scarcity of ion transport data in H_2O since, for instance, a drift tube-mass spectrometer (DTMS) experiment with mass analysis is limited in its operation to pressures less than 1 Torr [22]. Thus, we have obtained a self-consistent set of mobility and reaction rate data that explain the measurements over the E/N and gas pressure mentioned. Notwithstanding the above, it is important to confirm the present findings by other techniques in view of the great importance of these data in the understanding and modelling of atmospheric discharges and many other phenomena and applications in which water is involved. In particular, further insight into reaction (4), leading to OH^- formation, is strongly needed in view of the past and present discrepancies with the experimental values.

Acknowledgments

This work has been supported by Projects UNAM-PAPIIT IN111611 (México), MICINN AYA2011-29936-C05-02

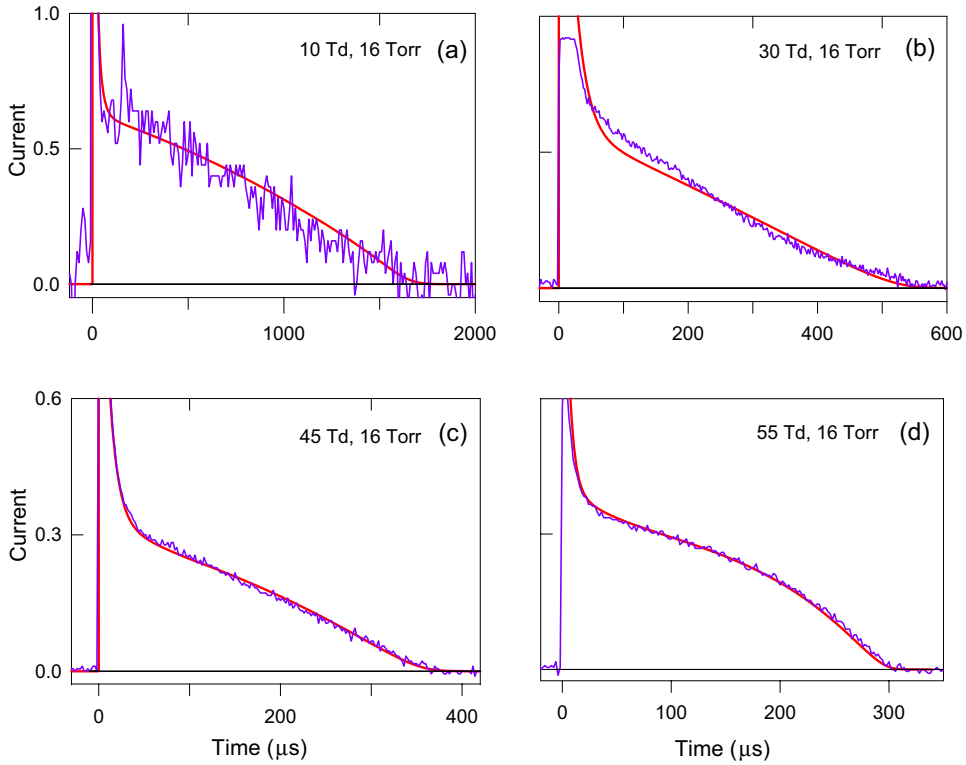

Figure 8. Negative-ion pulses in H_2O at the same pressure and varying E/N.

(Spain), and by the Junta de Andalucía, Proyecto de Excelencia FQM-5965 (Spain). G Ruíz-Vargas thanks Conacyt for a PhD grant and A Bekstein for a grant from PCF-UNAM. Thanks are due to A Bustos for his valuable technical assistance.

References

[1] Gordillo-Vázquez F J 2008 *J. Phys. D: Appl. Phys.* **41** 234016
[2] Bruggeman P and Schraam D C 2010 *Plasma Sources Sci. Technol.* **19** 045025
[3] Bekstein A, Benhenni M and Yousfi M 2011 *Eur. Phys. J.* D **61** 153 and references therein
[4] Viehland L A and Mason E A 1995 *At. Data Nucl. Data Tables* **60** 37
[5] de Urquijo J, Basurto E and Bekstein A 2011 *J. Phys. D: Appl. Phys.* **44** 325202 and references therein
[6] Muschlitz E E and Bailey T L 1956 *J. Phys. Chem.* **60** 681
[7] Schulz G J 1960 *J. Chem. Phys.* **33** 1661
[8] Moruzzi J L and Phelps A V 1966 *J. Chem. Phys.* **45** 4617
[9] Hasegawa H , Date H and Shimozuma M 2007 *J. Phys. D: Appl. Phys.* **40** 2495
[10] Lowke J D and Rees J A 1963 *Aust. J. Phys.* **16** 447
[11] Henson B L 1978 *J. Phys. D: Appl. Phys.* **11** 1405
[12] Melton C E 1972 *J. Chem. Phys.* **57** 4218
[13] Compton R N and Christophorou L G 1967 *Phys. Rev.* **154** 110
[14] Itikawa Y and Mason N J 2005 *J. Phys. Chem. Ref. Data* **34** 1
[15] Ruiz-Vargas G, de Urquijo J and Yousfi M 2010 *J. Phys. D: Appl. Phys.* **43** 455201
[16] Young L B, Lee-Ruff E and Bohme D K 1971 *Can. J. Chem.* **49** 979
Betowski D, Payzant J D, Mackay G I and Bohme D K 1975 *Chem. Phys. Lett.* **31** 321
Capitelli M, Ferreira C M, Gordiets B F and Osipov A I 2000 *Plasma Kinetics Kinetics in Atmospheric Gases* (Berlin: Springer)
Albritton D L 1978 *At. Data Nucl. Data Tables* **22** 1
[17] Moruzzi J L and Phelps A V 1966 *J. Chem. Phys.* **45** 4617
[18] Wilson J F, Davis F J, Nelson D R and Compton R N 1975 *J. Chem. Phys.* **62** 4204
[19] Hagelaar G J M and Pitchford L C 2005 *Plasma Sci. Sources Technol.* **14** 722
[20] Anicich V G 1993 *J. Phys. Chem. Ref. Data* **22** 1469
[21] Fritzenwallner J and Kopp E 1998 *Adv. Space Res.* **21** 891
[22] McDaniel E W and Mason E A 1973 *The Mobility and Diffusion of Ions in Gases* (New York: Wiley)
Mason E A and McDaniel E W 1988 *Transport Properties of Ions in Gases* (New York: Wiley)
[23] de Gouw J A, Krishnamurthy M and Leone S R 1997 *J. Chem. Phys.* **106** 5937
[24] Barker R A and Ridge D P 1976 *J. Chem. Phys.* **64** 4411
[25] de Urquijo J, Juárez A M, Rodríguez-Luna J C and Ramos-Salas J S 2007 *IEEE Trans. Plasma Sci.* **35** 1204
[26] Bekstein A, de Urquijo J, Hernández-Ávila J L and Basurto E 2012 *Eur. Phys. J.* D **66** 77